Fluid Dynamics Research



# Simulation of the mixing of a passive scalar in a round turbulent jet

To cite this article: C L Lubbers *et al* 2001 *Fluid Dyn. Res.* **28** 189

ELSEVIER

Fluid Dynamics Research 28 (2001) 189–208

FLUID DYNAMICS RESEARCH

# Simulation of the mixing of a passive scalar in a round turbulent jet

C.L. Lubbers, G. Brethouwer, B.J. Boersma *

*Laboratory for Aero- & Hydrodynamics, J.M. Burgers Centre, Delft University of Technology, 2628 AL Delft, The Netherlands*

Received 9 August 1999; received in revised form 10 April 2000; accepted 21 July 2000

**Abstract**

In this paper we present the results of the direct numerical simulation (DNS) of mixing of a passive scalar in a spatially developing free round turbulent jet. The Schmidt number used in the simulations is equal to 1.0 and the Reynolds number, based on the orifice diameter and velocity is equal to $2.0 \times 10^3$. The primary objective of this paper is to consider the self-similarity of the jet in the far field. Having considered the self-similarity of the velocity in a previous publication, we concentrate here on the self-similarity of the concentration of the passive scalar. To this end we have considered the profiles of the mean concentration and its fluctuations, together with the concentration probability density function distribution. The results have been compared with various experimental data that have been published in the literature. In general, the results agree very well with the experimental data. The conclusion is that the mean concentration is self-similar in the far field. The profiles of the root mean square of the concentration fluctuations are not self-similar. Furthermore, it is shown that the turbulent Schmidt number is equal to 0.74, which agrees very well with experimental values. © 2001 Published by The Japan Society of Fluid Mechanics and Elsevier Science B.V. All rights reserved.

*PACS:* 47.27.W

*Keywords:* Jets; Turbulent mixing

## 1. Introduction

The free round turbulent jet which results when fluid is issued from a circular orifice into free space, is one of the classical prototypes of turbulent free shear flows. Its simple geometry makes it an attractive subject for the study of turbulence. Many experimental investigations have been carried out to document the various turbulence characteristics of the jet flow. As examples we may mention here Panchapakesan and Lumley (1993) and Hussein et al. (1994). Jet flow has also been a subject of theoretical study and here attention has been mostly given to similarity theory. The premise of

* Corresponding author.
*E-mail address:* b.j.boersma@wbmt.tudelft.nl (B.J. Boersma).

0169-5983/01/$20.00 
PII: S0169-5983(00)00026-5

this theory is that, when properly scaled, flow variables such as the mean velocity profile can be expressed in terms of a unique function at each downstream distance along the jet axis. Although the similarity approach may seem straightforward, its application in particular to jet flow has not been without controversy, for a recent discussion we refer to Boersma et al. (1998).

Apart from its dynamics, turbulent jet flow has been also widely studied for its mixing properties. Together with the fluid flow one may also emit a substance from the orifice which is then dispersed by the turbulence. The substance is usually taken to be passive, which means that it does not contribute to the jet dynamics. It is thus carried along passively by the flow while being dispersed by the turbulence. Apart from a fundamental interest in the mixing processes within a turbulent jet, a study of jet mixing is also of much practical importance. For instance, jet flows in combination with turbulent mixing can be found in many industrial applications, e.g. fuel injectors in combustion engines, propulsion systems for aircraft and spacecraft but also many combustion flames can in essence be considered as turbulent mixing jets. To improve the efficiency of these processes and devices, it is important to gain more insight into the mixing of the jet fluid and the surrounding fluid and this will be the general objective of this paper.

Turbulent mixing in jet flow has been investigated by experimental methods in many studies. As an example we may mention here Corrsin and Uberoi (1950) who used a hot-wire anemometer to detect temperature fluctuations. Becker et al. (1967) investigated the concentration field of the round turbulent free jet. Later, Chevray and Tutu (1978) investigated intermittency in the temperature transport in a turbulent jet. They found that the turbulent Prandtl number is very different from unity and that it varies from location to location in the flow. Dowling and Dimotakis (1990) investigated the similarity of the concentration field at different Reynolds numbers. They found that the mean concentration profile is self-similar and independent of Reynolds number which they call general similarity. The root mean square of the fluctuations of the concentration and the probability density function of the concentration were found to be self-similar with a dependence of the Reynolds number which they call specific similarity. Scheffer et al. (1994) investigated the role of large-scale structure in the mixing of a non-reacting turbulent $CH_4$ jet. These structures result in instantaneous radial concentration profiles that differ considerably from the Gaussian-shaped mean profiles. They suggest a mixing model in which the dominant mechanism for entrainment is engulfment of the surrounding fluid by the large-scale vortical structures followed by rapid mixing with the jet fluid.

From a theoretical point of view mixing in a turbulent jet flow has been mainly treated in terms of self-similarity theory. The various details of this theory have been described in the papers mentioned above in connection with the analysis of experimental data. An overview of self-similarity of concentration profiles may be found in various textbooks such as Hinze (1975), Townsend (1976) and Schlichting (1979).

In addition to the experimental and theoretical studies on turbulent jet flow quoted above, it has recently become feasible to perform numerical simulations of this flow. Most of these numerical studies have concentrated on the initial phase of jet development where transition process occurs by which the laminar flow in the region close to the jet orifice turns into a turbulent flow. Examples of such studies are Brancher et al. (1994), Verzicco and Orlandi (1994) and Danaila et al. (1997). For the case of a fully developed jet, a numerical simulation study has been carried out by Boersma et al. (1998). To our knowledge turbulent mixing by a fully developed jet has not been treated by numerical simulations so far.

The objective of the present paper is to carry out a direct numerical simulation (DNS) of a turbulent jet in combination with the mixing of a passive scalar. Point of departure is the simulation by Boersma et al. (1998) which we extend by adding a transport equation for the mixing of a passive scalar. Our aim is to simulate the turbulent dispersion process starting from the orifice to within the similarity region of the jet. The simulations will be extensively compared with available experimental data. First we want to establish that a realistic DNS of the mixing process in a turbulent jet is feasible. Furthermore, we aim to use the simulation data to get more information and insight into the process of turbulent mixing. In particular, we intend to focus on the self-similarity properties of the various concentration statistics.

The outline of this paper is as follows. First, in Section 2 we will introduce the basic equations that describe the velocity and concentration distribution in a turbulent jet. In the same section we will discuss the principles of similarity theory. In Section 3, we will discuss the numerical method used for our turbulence simulation. Next, in Section 4 the results are compared with experimental data. Finally, the conclusions are given in Section 5.

## 2. Equations of motion and their self-similar solution

The velocity field of an incompressible turbulent jet is governed by the Navier–Stokes equations which read

$$\nabla \cdot \mathbf{u} = 0, \tag{1}$$

$$\frac{\partial \mathbf{u}}{\partial t} + \nabla \cdot (\mathbf{u}\mathbf{u}) = -\frac{1}{\rho}\nabla p + \nu \nabla^2 \mathbf{u}, \tag{2}$$

where $\mathbf{u}$ is the velocity vector, $p$ the pressure, and $\rho$ and $\nu$ are the density and kinematic viscosity of the fluid, respectively.

The passive scalar $c$ in this flow is governed by the following transport equation:

$$\frac{\partial c}{\partial t} + \nabla \cdot (\mathbf{u}c) = \mathbb{D}\nabla^2 c, \tag{3}$$

where $\mathbb{D}$ is the molecular diffusion coefficient. The ratio of the kinematic viscosity and the molecular diffusion coefficient $(\nu/\mathbb{D})$ is denoted as the Schmidt number.

The stationary and axisymmetric turbulent jet can be conveniently described with the help of a cylindrical coordinate system with $z$ as the axial coordinate directed along the jet axis and $r$ the radial coordinate. The $\bar{u}_z$ and $\bar{u}_r$ are the axial and radial components of the mean velocity. The equations for $\bar{u}_z$ and $\bar{u}_r$ can be obtained from (1) and (2) after some manipulation and after application of the so-called boundary-layer approximation (Hinze, 1975). The result reads

$$\frac{1}{r}\frac{\partial r\overline{u}_r}{\partial r} + \frac{\partial \overline{u}_z}{\partial z} = 0, \tag{4}$$

$$\overline{u}_r \frac{\partial \overline{u}_z}{\partial r} + \overline{u}_z \frac{\partial \overline{u}_z}{\partial z} = -\frac{1}{r}\frac{\partial}{\partial r} r\overline{u_r u_z}, \tag{5}$$

where $\overline{u_r u_z}$ denotes the covariance of the velocity fluctuations. We have neglected in (5) the contribution of the viscous terms based on the assumption that the Reynolds number is sufficiently high.

First we introduce a streamfunction $\psi$ which is defined by $\bar{u}_z = (1/r)\partial\psi/\partial r$ and $\bar{u}_r = -(1/r)\partial\psi/\partial z$, to integrate the continuity equation (5). Let us now consider a similarity solution of (5). This means that we look for solutions given by

$$u_z(r,z) = U_s(z)f(\eta), \quad \overline{u_r u_z} = \mathscr{U}^2(z)g(\eta), \quad \eta = \frac{r}{\mathscr{L}(z)}, \tag{6}$$

where $U_s$ is a scale for the mean velocity, $\mathscr{U}$ a scale for the velocity fluctuations and $\mathscr{L}$ a length scale. The $U_s$ is usually taken to be equal to the value of the mean velocity on the jet axis. The length scale $\mathscr{L}$ is frequently defined as the radial distance where the mean velocity is equal to half the centerline velocity. Given the definition of the streamfunction it then follows that

$$\psi(r,z) = U_s\mathscr{L}(z)^2F(\eta) \tag{7}$$

with $f(\eta) = F'(\eta)/\eta$.

Substitution of these expressions in (5) and using (4), leads to the following relation:

$$-\frac{U_s^2}{\mathscr{U}^2}\frac{\partial\mathscr{L}(z)}{\partial z}\left\{\left(\frac{F'}{\eta}\right)^2 + \frac{F}{\eta}\frac{\mathrm{d}}{\mathrm{d}\eta}\left(\frac{F'}{\eta}\right)\right\} = \frac{1}{\eta}\frac{\mathrm{d}}{\mathrm{d}\eta}(\eta g), \tag{8}$$

where we have also used conservation of axial momentum flux which can be derived by integrating (5) across a plane perpendicular to the jet axis and which leads to the relation $U_s\mathscr{L}(z) = \text{constant}$. Eq. (8) shows that similarity is only possible if

$$\frac{U_s^2}{\mathscr{U}^2}\frac{\partial\mathscr{L}(z)}{\partial z} = c_1, \tag{9}$$

with $c_1$ a constant. In view of the fact that the only constraint to be satisfied by the solution is conservation of momentum flux, (8) implies that the constant $c_1$ must be universal, i.e. independent of the flow details near the orifice.

To proceed some further assumptions must be made. The most straightforward one is to take $U_s = \mathscr{U}$ in (9) (see e.g. Tennekes and Lumley, 1972). It then follows immediately that

$$\frac{\partial\mathscr{L}(z)}{\partial z} = c_1 \tag{10}$$

which implies that the length scale is a universal function of $z$. In other words all jets have in their similarity region the same spreading rate irrespective of the initial conditions.

The existence of a universal spreading rate has been questioned by George (1989) who argues that there is no argument to assume that (10) is correct. He then proceeds by assuming $U_s \neq \mathscr{U}$ so that the spreading rate of a jet is not universal. The viewpoint of George seems to be supported by recent numerical simulations reported by Boersma et al. (1998) to which we refer for further discussion on the similarity of the mean velocity and also of turbulence statistics. Here, we will further concentrate on the similarity of the concentration profile.

Under the same assumptions as used for the derivation of (4) and (5) we can also obtain an equation for the mean concentration profile which reads

$$\bar{u}_r\frac{\partial\bar{c}}{\partial r} + \bar{u}_z\frac{\partial\bar{c}}{\partial z} = -\frac{1}{r}\frac{\partial}{\partial r}r\overline{u_r c}, \tag{11}$$

where again $\overline{u_r c}$ is the turbulent flux of the scalar and where the molecular diffusion term has been neglected based on the assumption of a sufficiently large Reynolds number.

Let us again look for a similarity solution given by

$$C(r,z) = C_s(z)h(\eta), \quad \overline{u_r c} = \mathscr{U}(z)\mathscr{C}(z)k(\eta), \quad \eta = \frac{r}{\mathscr{L}_c(z)}, \tag{12}$$

where $C_s$ is a scale for the mean concentration and $\mathscr{C}$ a scale for the concentration fluctuations. Similar to the velocity scale $U_s$, $C_s$ is taken equal to the mean concentration value at the jet axis. The $\mathscr{L}_c(z)$ is a length scale for the concentration profile which in principle does not have to be equal to the length scale for the velocity profile.

We first consider the consequences of conservation of concentration flux which can be derived from (11) by integration across a plane perpendicular to the jet axis and which reads

$$\int_0^\infty \bar{c}\,\bar{u}_z r\,\mathrm{d}r = \frac{Q_0}{2\pi}, \tag{13}$$

where $Q_0$ is the source strength of concentration introduced at the orifice. Substitution of the similarity solution (6) and (12) into (13) leads to the conclusion that similarity can only be satisfied when $\mathscr{L}_c(z) \simeq \mathscr{L}(z)$ and without loss of generality we take $\mathscr{L}_c(z) \equiv \mathscr{L}(z)$. One should realize however, that this choice means that at $r = \mathscr{L}(z)$ the mean concentration is not necessarily equal to half the centerline concentration. With this result for $\mathscr{L}_c(z)$ and with $U_s\mathscr{L} = \text{constant}$ we find from (13) that $C_s(z)\mathscr{L}(z)$ is also a constant.

Substituting the similarity expressions for mean concentration and the mean velocity profile into Eq. (11), we find after using the relationships between $U_s$, $C_s$ and $\mathscr{L}$ derived above, the following equation:

$$\frac{U_s\mathscr{C}}{C_s\mathscr{U}}\frac{\mathrm{d}}{\mathrm{d}\eta}(Fh) = \frac{\mathrm{d}}{\mathrm{d}\eta}(\eta k). \tag{14}$$

We see that similarity is only possible when

$$\frac{U_s\mathscr{C}}{C_s\mathscr{U}} = c_2 \tag{15}$$

with $c_2$ as another universal constant. Integrating (14) we get

$$\frac{Fh}{\eta k} = \frac{1}{c_2}, \tag{16}$$

where we have used the boundary condition that $F(0) = 0$. If we assume that $U_s = \mathscr{U}$ we find that $\mathscr{C}/C_s = c_2$ and hence the normalized scalar concentration in the far field is completely independent of the conditions at the jet nozzle. Previously, we stated that it is very unlikely that $U_s = \mathscr{U}$, thus $\mathscr{C} \neq c_2 C_s$ which implies that the scalar concentration in the far field, like the velocity field, depends on the conditions at the jet nozzle (see e.g. George, 1989; Boersma et al., 1998).

Finally, we consider the equation for the concentration variance $\overline{c^2}$ which in the boundary-layer approximation reads

$$\bar{u}_r\frac{\partial\overline{c^2}}{\partial r} + \bar{u}_z\frac{\partial\overline{c^2}}{\partial z} = -2\overline{cu_r}\frac{\partial\bar{c}}{\partial r} - \frac{\partial\overline{c^2u_r}}{\partial r} - \chi, \tag{17}$$

where we have again neglected transport by molecular diffusion. The molecular destruction of concentration fluctuations $\chi$ is defined as

$$\chi = 2\mathbb{D}\overline{\left(\frac{\partial c}{\partial x_j}\right)^2}, \tag{18}$$

where the index $j$ means a sum over all coordinate directions.

Let us again consider under which conditions (17) allows similarity solutions. To this end we introduce the following expressions:

$$\overline{c^2} = \mathscr{C}^2 m(\eta), \quad \overline{u_r c^2} = \mathscr{C}^2 \mathscr{U} n(\eta). \tag{19}$$

After substitution of these expressions in (17) and after some manipulation with the relationships that we have derived above, we find

$$2\frac{U_s \mathscr{L}}{\mathscr{U} C_s}\frac{\mathrm{d}\mathscr{C}}{\mathrm{d}z}\frac{F'm}{\eta} + \frac{\mathscr{C}\mathscr{L}}{C_s \mathscr{U}}\frac{\mathrm{d}U_s}{\mathrm{d}z}\frac{Fm'}{\eta} = -2kh' + \frac{\mathscr{C}}{C_s}n' - \frac{\mathscr{L}\chi}{\mathscr{U}\mathscr{C}C_s}. \tag{20}$$

This result shows that complete similarity of the variance of concentration fluctuations is only possible when $\mathscr{C} \simeq C_s$. If we substitute these results in (20) we find that full similarity requires additionally that $\mathrm{d}\mathscr{L}/\mathrm{d}z = \text{constant}$. This means that full similarity is only possible when the spreading rate of the jet is universal. As we have argued above that this result may be questionable, it seems that full similarity of the concentration variance profile cannot be expected.

## 3. Details of the direct numerical simulation

In this section we describe the details of the DNS of the round jet. The numerical procedure has already been described by Boersma et al. (1998) so that a short summary will suffice here. The DNS is based on a numerical solution of Eqs. (1)–(3) formulated in a spherical system. Such a coordinate system allows for a well-balanced numerical resolution both near the inflow as well as in the far field of the jet.

In this spherical coordinate system Eqs. (2) and (3) are discretized on a three-dimensional staggered grid with the help of a second-order finite volume method. The singularity at the centerline of the system is removed by the finite volume method because all the terms in the equations are multiplied by the Jacobian $r^2 \sin\theta$ (see e.g. Mohensi and Colonius, 2000). The grid is non-uniform in the radial direction which allows for accurate calculation near the orifice without using too many grid points in the far field. The time integration is carried out with a second-order Adams–Bashforth scheme. For the scalar field, the discretization is done with a monotone difference scheme. The monotone scheme is used to avoid 'wiggles' in the concentration field which may cause negative values or values higher than the source concentration, which are both physically unacceptable. The scheme has a local accuracy of at least $\mathscr{O}(h)$ and a global accuracy $\mathscr{O}(h^2)$, for more details we refer to Koren (1993) and Zijlema and Wesseling (1998).

Next we consider the boundary conditions. At the inflow boundary we impose a uniform profile for the velocity ($U_0$) and the concentration ($C_0$) at the orifice which has a diameter $D$. Outside the orifice the velocity and the concentration are set to zero. The pressure on the inflow plane is left free. At the side or lateral boundaries we use the so-called traction-free boundary condition for

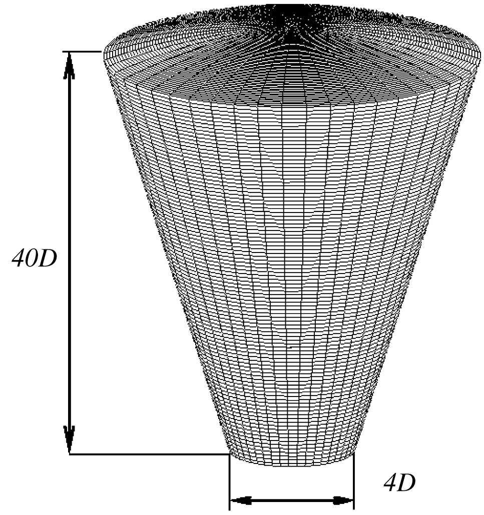


Fig. 1. A sketch of the computational grid.

the velocity (see Boersma et al., 1998). An advantage of this boundary condition is that a velocity across the boundary is allowed which is needed to accommodate the entrainment by the jet. For the concentration on the lateral boundary we set the gradient along the normal on this boundary equal to zero. At the outflow we use for the velocity and the concentration the so-called convective boundary conditions (Akselvoll and Moin, 1996).

The domain is a part of the spherical shell (see Fig. 1) with its radius between $51D$ and $91D$ and with a limiting angle of $\pi/40$. The grid that we used for our computations consists of $400 \times 80 \times 96$ grid points in the radial ($r$), tangential ($\theta$) and the azimuthal ($\phi$) direction, respectively. This resolution is comparable to the one used by Boersma et al. (1998). In this paper it has been proven that the resolution is sufficient to resolve all important scales of motions. The Reynolds number which is defined as $\mathrm{Re} = DU_0/\nu$ is $2.0 \times 10^3$ and the Schmidt number which is defined as $\mathrm{Sc} = \nu/\mathbb{D}$ is 1. The calculations are performed on a Cray-J90se parallel vector computer. The code takes 52Mwords of memory and one time step takes approximately 33 CPU seconds.

For the statistical analysis we have stored 40 three-dimensional data fields which are separated in time by $2D/U_{\text{orifice}}$. The statistics are obtained by averaging in the circumferential direction and in time.

## 4. Results and discussion

In this section, the results of the DNS of the velocity field of the turbulent jet, as well of the passive scalar are presented.

To present the results, we will use a cylindrical coordinate system in the sequel of this paper because all the experimental studies use such a system. All results are obtained by averaging over several data fields and over the self-similarity coordinate $\eta = r/(z - z_0)$ or $\eta = r/r_{1/2}$ in the region $20D < z < 37.5D$, where now $r$ is the radial distance to the centerline, $z$ is the distance to the

Table 1
Data of some experiments

| Author | Re | Sc or Pr |
|---|---|---|
| Panchapakesan and Lumley (1993) | 11,000 | — |
| Hussein et al. (1994) | $10^5$ | — |
| Becker et al. (1967) | 54,000 | 38,000 |
| Birch et al. (1978) | 16,000 | 0.70 |
| Lockwood and Moneib (1980) | 50,000 | 0.70 |
| Dahm and Dimotakis (1987) | 5000 | 600–800 |
| Chua and Antonia (1990) | 17,700 | 0.70 |
| Chevray and Tutu (1978) | $3.8 \times 10^6$ | 0.70 |
| Dowling and Dimotakis (1990) | 5000 | 1.0 |
| Present | 2000 | 1.0 |

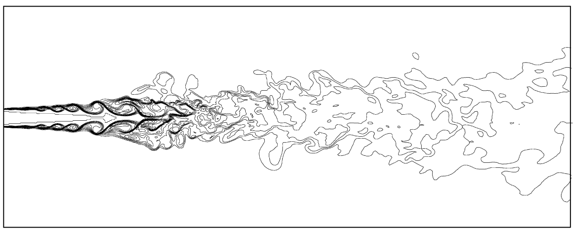


Fig. 2. An iso-contour plot of the concentration (15 contour levels equally spaced from 0.07 to 1).

orifice, $z_0$ is the distance of the virtual origin to the orifice and $r_{1/2}$ denotes the radial distance, where the local mean axial velocity is equal to half the value of the mean centerline velocity, i.e. $\bar{U}(r_{1/2}) = \bar{U}_c/2$. We do not use the statistics of the last 2.5 diameters of the domain, because of the possible influences of the outflow boundary condition. In George (1989) it has been discussed that using $\eta = r/(z - z_0)$ is valid only when the jet spreads linearly.

First, we will show an instantaneous plot of the concentration field of the jet in the axial direction. Second, we present the results of the statistics of the velocity profiles to show that the velocity field is in good agreement with experimental data. Then we will discuss the statistics of the concentration. All the results are compared with experimental data, which are summarized in Table 1. The results are presented in non-dimensional form. The velocity and concentration are scaled with the entrance or the centerline value, depending on whether we are interested in the downstream development or cross-stream profiles, respectively. The axial coordinate is scaled with the jet orifice diameter $D$ and the radial coordinate with $r_{1/2}$ or $z - z_0$.

In Fig. 2 an iso-contour plot of the instantaneous concentration distribution in the jet in the axial direction is shown. The figure shows a laminar flow field close to the inflow plane of the jet. Farther downstream, the laminar vortex sheet rolls up due to the Kelvin–Helmholtz instability and the flow becomes turbulent.

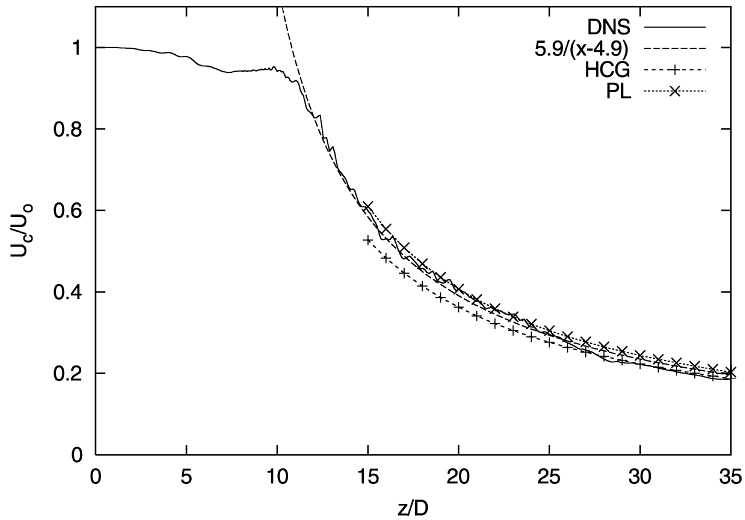


Fig. 3. Scaled centerline velocity $\bar{U}_c/U_0$ as a function of the distance to the orifice of the jet, obtained from DNS and from the experiments of Panchapakesan and Lumley (1993), and Hussein et al. (1994).

### 4.1. Mean velocity and turbulent statistics

In this section the flow field obtained from the DNS will be compared with the experimental data of Panchapakesan and Lumley (1993) and Hussein et al. (1994). We will show here only a few results as a more detailed validation of the DNS for the velocity statistics is given by Boersma et al. (1998).

In Fig. 3 we show the mean centerline velocity as a function of the distance to the orifice. In this figure we also show the curve fits given in the experimental papers by Hussein et al. (1994), and Panchapakesan and Lumley (1993). The agreement between the simulation and the curve fits given in the experimental papers is very good.

Next in Fig. 4 we show the mean velocity profile versus the self-similarity coordinate $\eta = r/[z - z_0]$ together with experimental data obtained by Panchapakesan and Lumley (1993). Fig. 5 shows the Reynolds shear stress as a function of $\eta$ again with experimental data obtained by Panchapakesan and Lumley (1993). Both figures show excellent agreement between DNS and experiment. This gives us a good starting point to study turbulent mixing in more detail.

### 4.2. Concentration profiles

In the previous section, we have demonstrated that the simulated velocity field is in very good agreement with experimental results. In this section, we turn to the turbulent mixing in the far field of the jet. The statistics of the DNS are again computed in the region $20D < z < 37D$. It is assumed that in this region the statistics are self-similar. First, the mean concentration profiles are presented and then the rms and the probability density functions of the concentration fluctuations. The results are compared with experimental data.

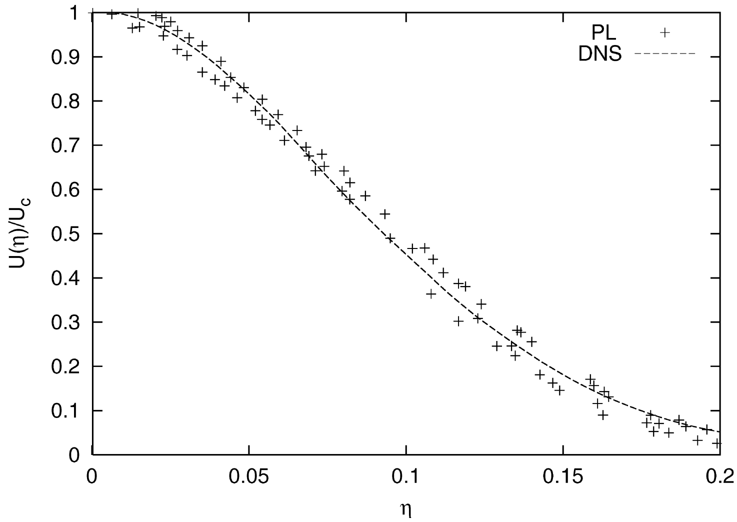


Fig. 4. Mean axial velocity as a function of the self-similarity coordinate $\eta$. Solid line DNS, symbols experimental values of Panchapakesan and Lumley (1993).

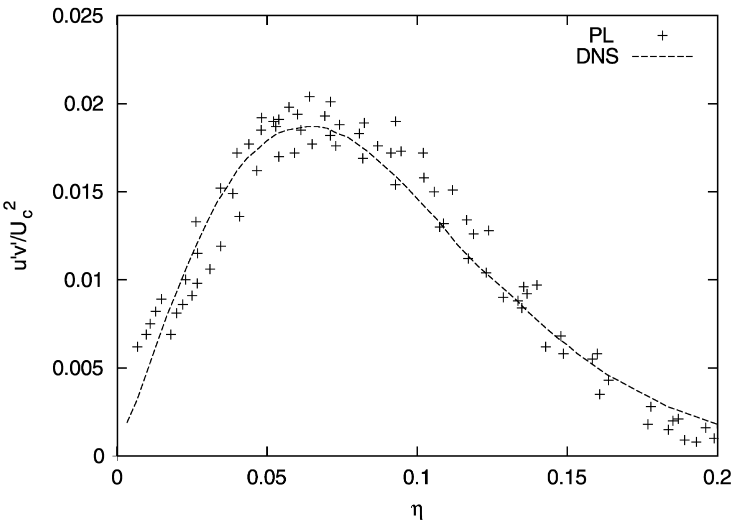


Fig. 5. Reynolds shear stress as a function of the self-similarity coordinate $\eta$. Solid line DNS, symbols experimental values of Panchapakesan and Lumley (1993).

### 4.2.1. *Mean concentration*

In Fig. 6, the mean axial centerline velocity $\bar{U}_c$ and the centerline mean concentration $\bar{C}_c$, scaled with the values at the orifice, are plotted versus the distance to the orifice. This figure shows that the values of the concentration and the axial velocity are constant in the initial laminar part of the jet. After the transition to a turbulent jet, the profiles collapse to a curve proportional to $z^{-1}$. We note that the mean concentration decays faster than the mean velocity.

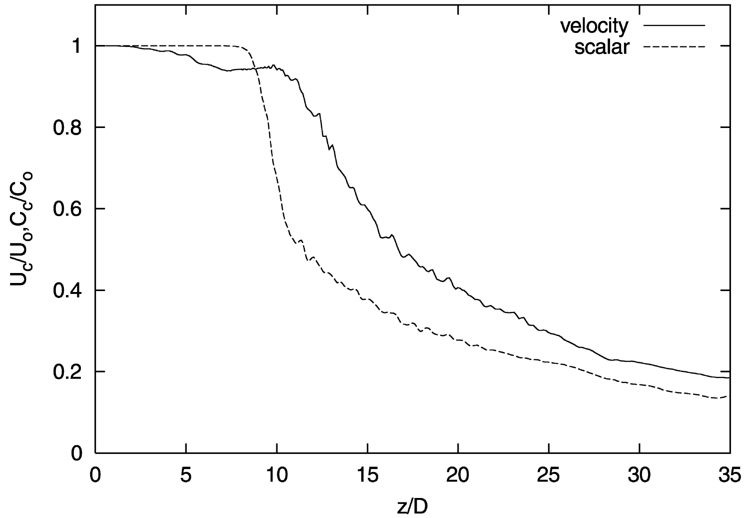


Fig. 6. The mean axial velocity at the centerline and the centerline mean concentration as a function of the axial coordinate. Both curves are normalized with the orifice value.

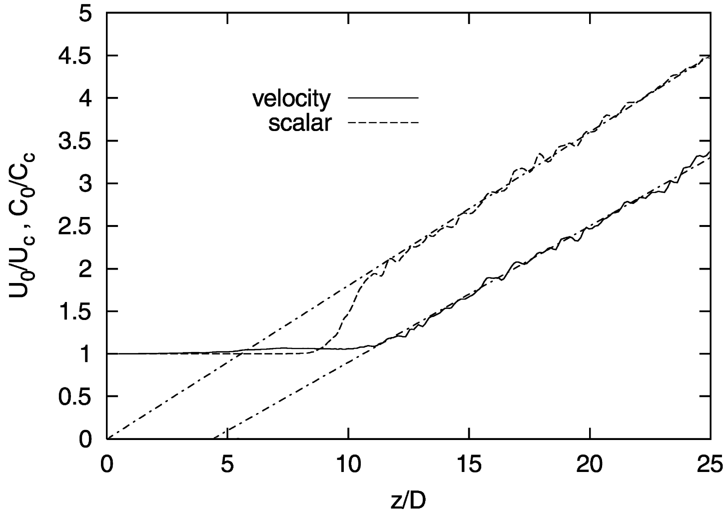


Fig. 7. The inverse of the mean axial velocity and mean concentration as a function of the axial coordinate. The straight lines are fits for the far field. For the velocity $x/6.1$ and for the scalar $x/5.5$.

If the spreading of the jet is linear, the reciprocal of the centerline velocity and concentration should produce straight lines. They are plotted in Fig. 7 and both curves fit very well to a straight line. In order to know the values of the decay constants $\kappa_u, \kappa_c$, we have fitted the data shown in Fig. 7 to the following equations:

$$\frac{U_c}{U_0} = \kappa_u \left[\frac{D}{z - z_0}\right] \quad \text{and} \quad \frac{C_c}{C_0} = \kappa_c \left[\frac{D}{z - z_0}\right], \tag{21}$$

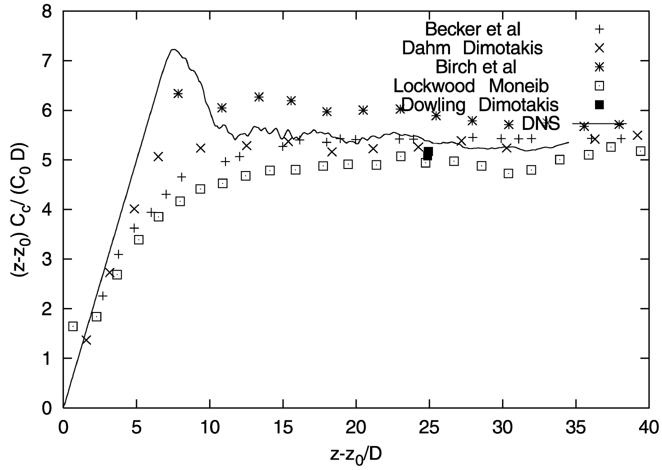


Fig. 8. $(z-z_0)C_c/(C_0D)$ versus the distance to the virtual origin $(z-z_0)/D$, obtained from DNS (solid line) and experiments of Lockwood and Moneib (1980), Dahm and Dimotakis (1987), Becker et al. (1967), Dowling and Dimotakis (1990), and Birch et al. (1978).

where $z_0$ is the virtual origin of the jet and $\kappa_u$ and $\kappa_c$ the mean decay constants for the velocity and scalar, respectively. We find that for our DNS the decay constant $\kappa_c$ (concentration) is 5.5 with a virtual origin of $z_0 = 0.5D$. For the velocity we find $\kappa_u = 6.1$ with a virtual origin $z_0 = 5.5D$.

In Fig. 8, we show $(z - z_0)C_c/(DC_0)$, as a function of the distance to the jet orifice. Also plotted in this figure are the experimental values obtained by Lockwood and Moneib (1980), Dahm and Dimotakis (1985), Becker et al. (1967), Dowling and Dimotakis (1988), and Birch et al. (1978). In the experiments $(z - z_0)C_c/(DC_0)$, has in general a value between 4 and 6 depending on the experimental setup. We see that the value that we have computed from our DNS, lies in between these values. Because the value of $(z - z_0)C_c/(DC_0)$ is fairly constant, we may conclude that the mean concentration shows *general* similarity. There seems to be no connection between the value of $(z - z_0)C_c/(DC_0)$ and the value of the Reynolds number or Schmidt number. Only the initial conditions may still have an influence on the value of this constant.

Next in Fig. 9 we show the mean concentration profile obtained from the simulations normalized with the mean concentration at the centerline as a function of the non-dimensional radial coordinate $\eta = r/(z - z_0)$. We assume that the mean scalar concentration reaches self-similarity after $20D$ from the jet orifice. Therefore, the statistics of the mean concentration have been taken in the region $20D < z < 37D$. Fig. 9 also shows the experimental data obtained by Dowling and Dimotakis (1990) at Re=5000 and at various distances of the orifice of the jet, i.e. $20D$, $40D$, $60D$, $80D$. The half-width value $\eta_{1/2}$ for the mean concentration profile in our simulations, i.e. the value of $r/(z - z_0)$ where $\bar{C}/\bar{C}_c = 0.5$, is 0.112. When we assume that the mean concentration profile is Gaussian, i.e.

$$\frac{\bar{C}(\eta)}{\bar{C}_c} = \exp(-K_c\eta^2) \qquad (22)$$

and when we use the value for the half-width given above, we obtain $K_c = 55.3$. If we use a least-squares fit through the DNS data, we find the best agreement between our results and the

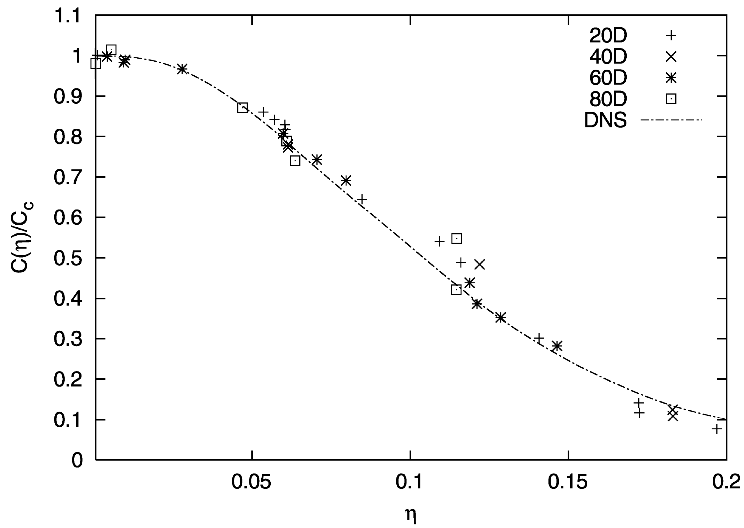


Fig. 9. The mean concentration profile versus the self-similarity coordinate $\eta$, from DNS (line) and the experiment of Dowling and Dimotakis (1990) (symbols).

Gaussian profile for $K_c = 56.6$. The best least-squares fit through all points of the experimental data gives $K_c = 59.1$. The half-width value $\eta_{1/2}$ where $\bar{C} = \bar{C}_c/2$ is then 0.108. These results seem consistent and are in good agreement with our data. We, therefore, conclude that the mean concentration is self-similar and independent of the Reynolds number. This implies that the mean concentration profile displays *general* self-similarity along rays that emanate from the virtual origin of the jet. When we compare the value $K_c = 55.3$ with $K_u = 76.2$ which we found for the axial velocity, it follows that the concentration field is wider than the velocity field. In other words the concentration field spreads faster than the velocity field. That the concentration spreads faster than the axial velocity is associated with the preferential transport of the scalar over momentum. Concluding we can say that the results of our simulations are in excellent agreement with the experimental data of Dowling and Dimotakis (1990) and that the mean concentration profiles are self-similar.

#### 4.2.2. Fluctuation of the concentration

In Fig. 10, we show the rms of the concentration fluctuations normalized with the centerline mean concentration as a function of $\eta = r/(z - z_0)$. In general it is assumed, that rms profiles reach only self-similarity beyond $20 - 25D$. Here, we have computed the statistics from the simulations data for the region $20D < z < 35D$. This may imply that the scaled rms profiles have not yet completely reached self-similarity. Fig. 10 also shows the experimental data of Dowling and Dimotakis (1990). They measured at $z = 20D, 40D, 60D$ and $80D$ and at Reynolds $= 5000$. The results of the DNS are in reasonable agreement with these experimental measurements.

Fig. 11 illustrates the value of the rms of the concentration fluctuations at the centerline of the jet, normalized with the mean centerline concentration plotted against $(z - z_0)/D$. The peak at $z = 9D$ in the rms profile corresponds to the point where the centerline concentration starts to drop, e.g. Fig. 6.

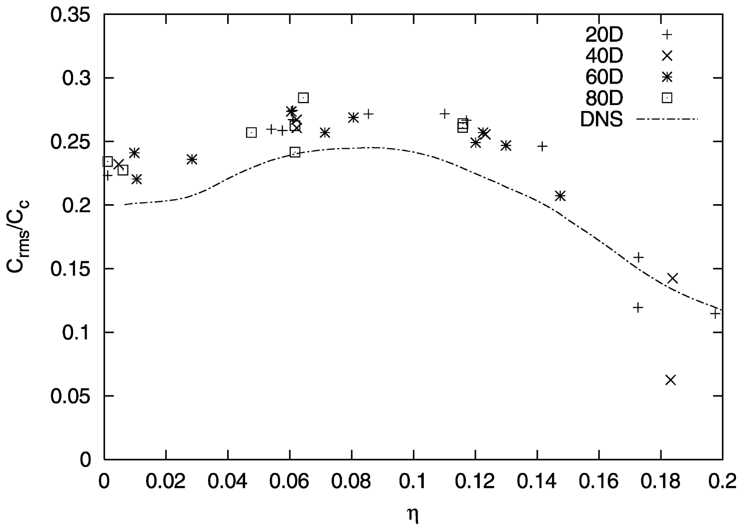


Fig. 10. Scaled rms value of the concentration $c_{\rm rms}/\bar{C}_{\rm c}$ as a function of the radial coordinate $\eta = r/(z - z_0)$, obtained from the DNS (solid line) and experiments of Dowling and Dimotakis (1990) (symbols).

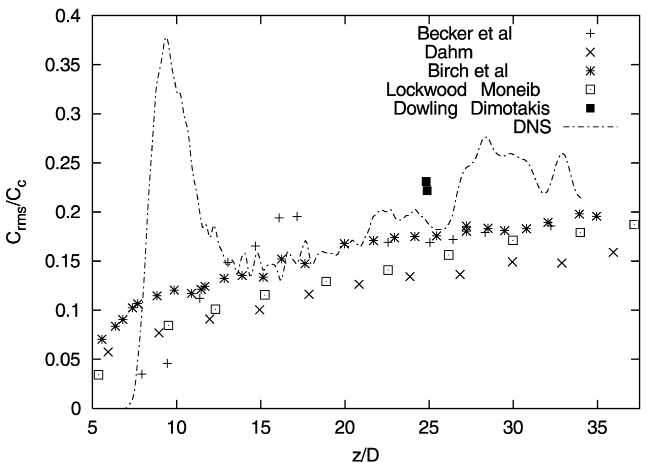


Fig. 11. Centerline rms scaled with the centerline concentration as a function of the distance to the orifice of the jet, obtained from DNS (solid line) and experiments of Lockwood and Moneib (1980), Dahm and Dimotakis (1985), Birch et al. (1978), Becker et al. (1967), and Dowling and Dimotakis (1990).

In Fig. 11 we have also plotted the experimental data of Lockwood and Moneib (1980), Dahm and Dimotakis (1985), Birch et al. (1978), Becker et al. (1967), and Dowling and Dimotakis (1988). The plots should approach a horizontal line when $c_{\rm rms}/\bar{C}_{\rm c}$ is self-similar. There is considerable scatter in the results of the simulations, but it is seen that the normalized rms of the scalar fluctuations keeps increasing with the downstream distance like most of the experimental data shown in Fig. 11.

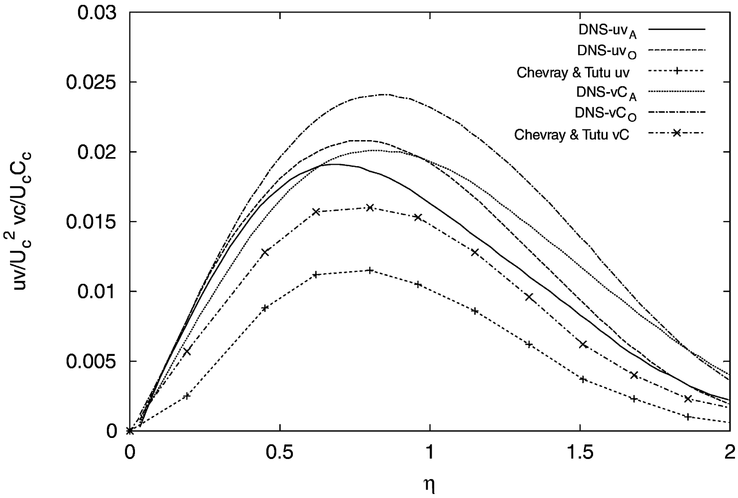


Fig. 12. The Reynolds stress and the turbulent concentration flux are plotted against the radial coordinate $\eta = r/r_{1/2}$, obtained from DNS (lines) and experiments of Chevray and Tutu (1978) (pointed line).

Dowling and Dimotakis found that the value of $c_{\rm rms}/\bar{C}_{\rm c}$ is 0.230 and 0.237 for Re $= 5000$ and 16,000, respectively. Based on this, they conclude that $c_{\rm rms}/\bar{C}$ has a *general* self-similar value on the centerline between 0.23 and 0.24. This is not supported by our DNS and also not by the other experimental results shown in Fig. 11. At the end of Section 2 we already argued that full self-similarity of the concentration variance is unlikely from a theoretical point of view and this seems to be supported by our DNS results and the experimental observations shown in Fig. 11.

### 4.2.3. Reynolds stress and turbulent concentration flux

In Fig. 12, the turbulent concentration flux $\overline{u_r c}$ in radial direction normalized with the mean velocity times mean concentration at the centerline is plotted as a function of $\eta = r/r_{1/2}$ together with the Reynolds stress $\overline{u_r u_z}$ normalized with the square of the centerline mean velocity. Fig. 12 also shows the experimental data of Chevray and Tutu (1978) who have investigated a turbulent jet at Re$=3.8\times10^6$. The results of the DNS show a larger Reynolds shear stress and turbulent concentration flux than the experimental results. Boersma et al. (1998) showed that the similarity profiles of $\overline{u_r u_z}$ can depend on the initial condition. In particular they showed that scaling $\overline{u_r u_z}$ with $U_{\rm c}^2 \partial\delta_{1/2}/\partial z$ gives better results, where $\partial\delta_{1/2}/\partial z$ is the decay of the jet half-width. Hill et al. (1976) showed that jets with laminar initial boundary layers have faster mixing rates, a much more prominent large-scale structure and a more rapid centerline velocity decay than those with an initially turbulent boundary layer. This is consistent with the lower values of the experimental data of Chevray and Tutu (1978) who probably had an initially turbulent boundary layer and therefore a lower decay constant. Scaling in the way Boersma et al. (1998) did, would therefore improve the agreement between the curves of the experimental data of Chevray and Tutu (1978) and ours.

The results of the simulations show also that the non-dimensional Reynolds shear stress is smaller than the turbulent concentration flux. The experimental data support this result. The turbulent flux

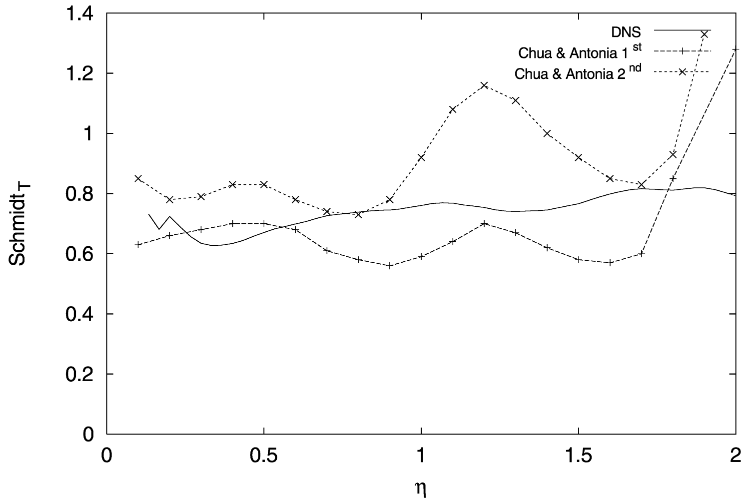


Fig. 13. The turbulent Schmidt number is plotted versus the radial coordinate $\eta = r/r_{1/2}$, obtained from the DNS (solid line) and experiments of Chua and Antonia (1990) measured with two different methods (pointed line).

$\overline{vc}/\bar{U}_c\bar{C}_c$ is larger than $\overline{uv}/\bar{U}_c^2$ because the transport of a scalar is more efficient than the transport of momentum. The reason for this is that in the momentum equation a pressure gradient is present which suppresses turbulent transport. Such a term is not present in the scalar transport equations. This result is consistent with the fact that the turbulent Schmidt number, i.e.

$$\mathrm{Sc_T} = \frac{\nu_\mathrm{T}}{\mathbb{D}_\mathrm{T}} \tag{23}$$

is smaller than unity. The Schmidt number, is plotted in Fig. 13. In this figure we also show the experimental data of Chua and Antonia (1990) who have used temperature as a tracer so that the equivalent of the Schmidt number in their case is the Prandtl number. Our results show far less fluctuations than those of experiment. Chua and Antonia (1990) used two different experimental methods. With their first method they found that over the range $0.1 < \eta < 1.0$ the turbulent Prandtl number is approximately constant with a value of 0.81. With their second method they found a value of 0.65. We find from the DNS a turbulent Schmidt number of 0.74 (averaged over the whole curve). Experimental values between 0.71 and 0.76 are reported by Chevray and Tutu (1978). So it seems that our result for the turbulent Schmidt number agrees reasonably well with the existing experimental data.

### 4.3. Probability density function of the concentration

In this section, we will discuss the probability distribution of the concentration in the jet at three different places in the self-similarity region. A histogram of the instantaneous concentration divided

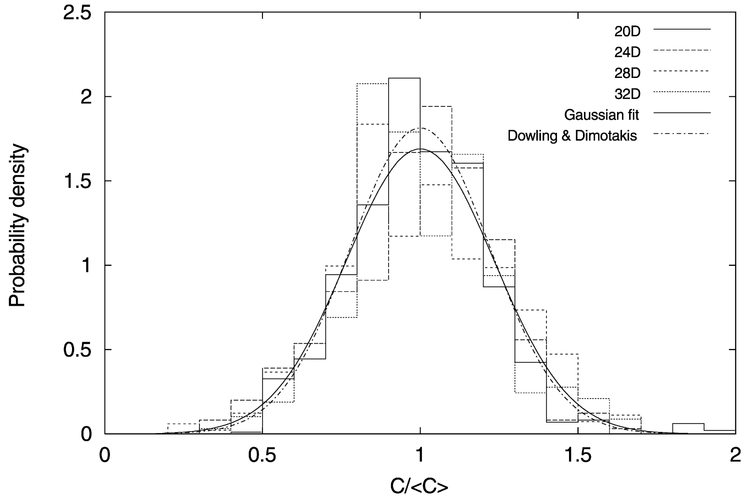


Fig. 14. Probability density function of the scaled concentration, $C/\bar{C}$, on the jet centerline at $z = 20D, 24D, 28D, 32D$, obtained from DNS and a Gaussian fit of the DNS and a Gaussian fit of the experimental data of Dowling and Dimotakis (1990).

by the local mean concentration, $C/\bar{C}$, was made by sorting the data into bins. The histogram was normalized, i.e.

$$\int_0^\infty \mathrm{PDF}(C/\bar{C})\,\mathrm{d}(C/\bar{C}) = 1, \tag{24}$$

to form a probability density function of the concentration. The independent variable $C/\bar{C}$, is chosen because dividing $C$ by $\bar{C}$ should remove the effect of the downstream decay of the mean concentration.

Fig. 14 shows the PDF on the jet centerline. This PDF shows some fluctuations due to the few independent samples especially near the centerline. Still, the distribution of the concentration seems Gaussian. The various histograms lie around a Gaussian fit, which is also included in the figure. In Fig. 14 we have also plotted the result of a Gaussian fit through the measured PDFs of Dowling and Dimotakis (1990) at $\mathrm{Re} = 5000$. The curve fitted through the DNS data has a smaller maximum and is a little wider than the curve of Dowling and Dimotakis (1990).

In Fig. 15, we have plotted the PDF along the ray $\eta = 0.06$. We also show a Gaussian curve fitted through the DNS data together with a Gaussian fit through the experimental data of Dowling and Dimotakis at $\mathrm{Re} = 5000$. The curve of the experimental data of Dowling and Dimotakis has in this case a smaller maximum and is a little wider than the curve fitted through the DNS data.

Fig. 16 illustrates the PDF along the ray $\eta = 0.12$. Here we see a broadening of the PDF profile with respect to the two other values of $\eta$. The profile deviates from a Gaussian profile so that at $\eta = 0.12$ the PDF can no longer be approximated by a Gaussian profile. When $\eta$ increases, the PDF changes from a Gaussian shape to a much flatter shape and the probability of zero concentration increases.

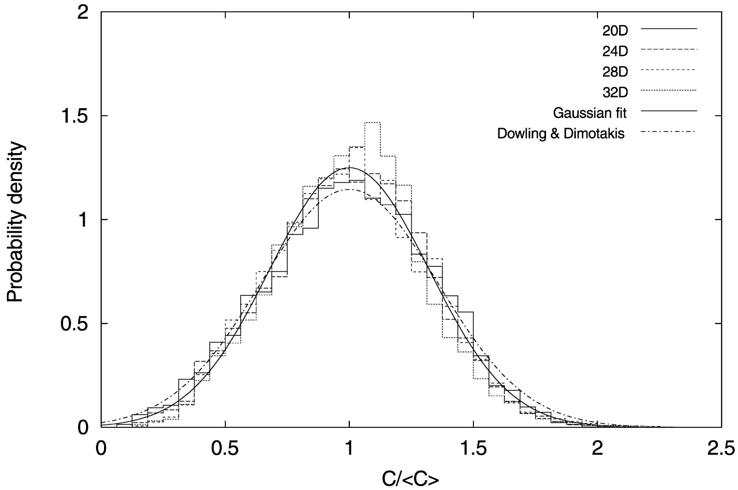


Fig. 15. Probability density function of the scaled concentration, $C/\bar{C}$, along ray $\eta = 0.06$ at $z = 20D, 24D, 28D, 32D$, obtained from DNS and a Gaussian fit of the DNS and a Gaussian fit of the experimental data of Dowling and Dimotakis (1990).

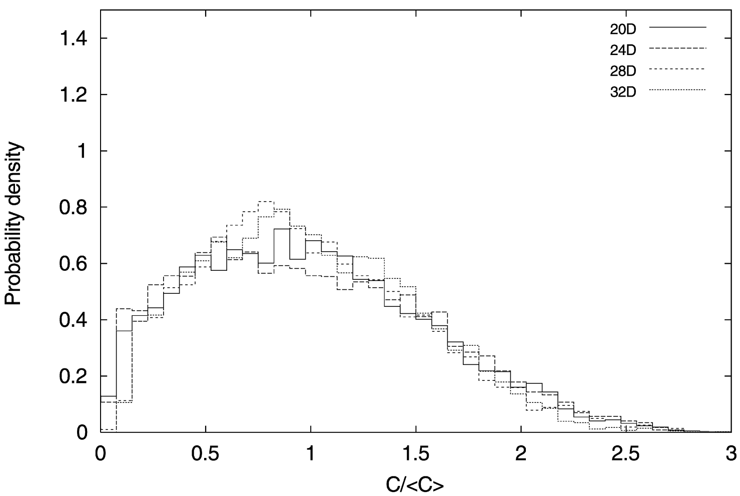


Fig. 16. Probability density function of the scaled concentration, $C/\bar{C}$, along ray $\eta = 0.12$ at $z = 20D, 24D, 28D, 32D$, obtained from DNS and a Gaussian fit.

## 5. Conclusion

In this paper we have presented some results obtained from the direct numerical simulation of a passive scalar in a turbulent jet. In general, the results show good agreement with existing experimental data. It is found that the mean concentration profiles are self-similar in agreement with experimental data. The variance of the concentration fluctuations is found to be not self-similar. This is in contrast with the results of Dowling and Dimotakis (1990) who claim that this variance is also self-similar. However, other experimental data are consistent with our results and show that the variance of the concentration fluctuations is not self-similar. Moreover, self similarity is also unlikely from a theoretical point of view.

## Acknowledgements

We would like to thank HP$\alpha$C (TU-Delft) for the CPU-time on the CRAY-J90 vector computer.

## References

Akselvoll, K., Moin, P., 1996. Large-eddy simulation of turbulent confined coannular jets. J. Fluid Mech. 315, 387–411.
Becker, H.A., Hottel, H.C., Williams, G.C., 1967. The nozzle fluid concentration field of the round turbulent jet. J. Fluid Mech. 30, 285–301.
Birch, A.D., Brown, D.R., Dodson, M.D., Thomas, J.R., 1978. The turbulent concentration field of a methane jet. J. Fluid Mech. 88, 431–449.
Boersma, B.J., Brethouwer, G., Nieuwstadt, F.T.M., 1998. A numerical investigation on the effect of the inflow conditions on the self-similar region of a round jet. Phys. Fluids 10, 899–909.
Brancher, P., Chomaz, J.M., Huerre, P., 1994. Direct numerical simulations of round jets: vortex induction and side jets. Phys. Fluids 6, 1768.
Chevray, R., Tutu, N.K., 1978. Intermittency and preferential transport of heat in round jet. J. Fluid Mech. Part 1 88, 133–160.
Chua, L.P., Antonia, R.A., 1990. Turbulent Prandtl Number in a circular jet. Int. J. Heat Mass Transfer 33 (2), 331–339.
Corrsin, S., Uberoi, M.S., 1950. Further experiments on the flow and heat transfer in a heated turbulent air jet. NACA Report 998.
Dahm, W.J.A., Dimotakis, P.E., 1987. Measurements of entrainment and mixing in turbulent jets. AIAA J. 25, 1216–1223.
Danaila, I., Dusek, J., Anselmet, F., 1997. Coherent structures in a round, spatially evolving, unforced, homogeneous jet at low Reynolds numbers. Phys. Fluids 9, 3323.
Dowling, D.R., Dimotakis, P.E., 1990. Similarity of the concentration field of gas-phase turbulent jets. J. Fluid Mech. 218, 109–141.
George, W.K., 1989. Self-preservation of turbulent flows and its relation to initial conditions and coherent structures. In: George, W.K., Arndts, R. (Eds.), Adv. Turbulence. Springer, Berlin.
Hill, W.J., Jenkins, R.C., Gilbert, B.L., 1976. Effects of the initial boundary-layer state in turbulent jet mixing. AIAA J. 14, 1513–1514.
Hinze, J.O., 1975. Turbulence. McGraw-Hill, New York.
Hussein, H.J., Capp, S.P., George, W.K., 1994. Velocity measurements in a high Reynolds number, momentum-conserving, axisymmetric, turbulent jet. J. Fluid Mech. 258, 31–76.
Koren, B., 1993. A robust upwind discretization method for advection, diffusion and source terms. In: Vreugdenhill, C.B., Koren, B. (Eds.), Numerical Methods for Advection-Diffusion Problems, Notes on Numerical Fluid Mechanics, Vol. 45. Vieweg, Braunschweig, pp. 117–138.
Lockwood, F.C., Moneib, H.A., 1980. Fluctuating temperature measurements in a heated round free jet. Combin. Sci. Technol. 22, 63–81.
Mohensi, K., Colonius, T., 2000. Numerical treatment of polar coordinate singularities. J. Comput. Phys. 157, 787–795.
Panchapakesan, N.R., Lumley, J.L., 1993. Turbulence measurements in axisymmetric jets of air and helium. Part 1. Air jet. J. Fluid Mech. 246, 197–224.
Scheffer, R.E., Kerstein, A.R., Namazian, M., Kelly, J., 1994. Role of large-scale structure in a nonreacting turbulent CH4 jet. Phys. Fluids 6, 652–661.
Schlichting, H., 1979. Boundary-Layer Theory, 7th Edition. McGraw–Hill, New York.

Tennekes, H., Lumley, J.L., 1972. A first course in turbulence. The MIT Press, Cambridge, MA.
Townsend, A.A., 1976. The Structure of Turbulent Shear Flow. Cambridge University Press, Cambridge.
Verzicco, R., Orlandi, P., 1994. Direct simulations of the transitional regime of a circular jet. Phys. Fluids 6, 751–759.
Zijlema, M., Wesseling, P., 1998. Higher-order flux-limiting schemes for the finite volume computation of incompressible flow. Int. J. Comput. Fluid Dyn. 9, 89–109.